Moving-mesh cosmology: properties of gas discs

Monthly Notices
of the
ROYAL ASTRONOMICAL SOCIETY

Mon. Not. R. Astron. Soc. **427,** 2224–2238 (2012) doi:10.1111/j.1365-2966.2012.22082.x

Moving-mesh cosmology: properties of gas discs

Paul Torrey,[1⋆] Mark Vogelsberger,[1] Debora Sijacki,[1†] Volker Springel[2,3] and Lars Hernquist[1]

[1]*Harvard–Smithsonian Center for Astrophysics, 60 Garden Street, Cambridge, MA 02138, USA*
[2]*Heidelberg Institute for Theoretical Studies, Schloss-Wolfsbrunnenweg 35, D-69118 Heidelberg, Germany*
[3]*Zentrum für Astronomie der Universität Heidelberg, ARI, Mönchhofstr. 12–14, D-69120 Heidelberg, Germany*

Accepted 2012 September 7. Received 2012 September 6; in original form 2012 July 18

ABSTRACT

We compare the structural properties of galaxies formed in cosmological simulations using the smoothed particle hydrodynamics (SPH) code GADGET with those using the moving-mesh code AREPO. Both codes employ identical gravity solvers and the same subresolution physics but use very different methods to track the hydrodynamic evolution of gas. This permits us to isolate the effects of the hydro solver on the formation and evolution of galactic gas discs in GADGET and AREPO haloes with comparable numerical resolution. In a matching sample of GADGET and AREPO haloes, we fit simulated gas discs with exponential profiles. We find that the cold gas discs formed using the moving-mesh approach have systematically larger disc scale lengths and higher specific angular momenta than their GADGET counterparts across a wide range in halo masses. For low-mass galaxies, differences between the properties of the simulated galaxy discs are caused by an insufficient number of resolution elements which lead to the artificial angular momentum transfer in our SPH calculation. We however find that galactic discs formed in massive haloes, resolved with $\geq 10^6$ particles/cells, are still systematically smaller in the GADGET run by a factor of $\sim$2. The reason for this is twofold: (i) the excessive heating of haloes close to the cooling radius due to spurious dissipation of the subsonic turbulence in GADGET reduces the supply of gas which can cool and settle on to the central disc; (ii) the efficient delivery of low angular momentum gaseous blobs to the bottom of the potential well results in the centrally concentrated gas discs in GADGET simulation. While this large population of gaseous blobs in GADGET originates from the filaments which are pressure confined and fragment due to the SPH surface tension while infalling into hot halo atmospheres, it is essentially absent in the moving-mesh calculation, clearly indicating numerical rather than physical origin of the blob material.

Key words: methods: numerical – Galaxy: formation – cosmology: theory.

1 INTRODUCTION

A primary goal of cosmological simulations is to self-consistently reproduce the variety of galaxy morphologies observed in the local Universe. While the formation of dark matter haloes via gravitational collapse has been simulated in great detail using *N*-body simulations (e.g. Springel et al. 2005; Fosalba et al. 2008; Boylan-Kolchin et al. 2009; Teyssier et al. 2009; Klypin, Trujillo-Gomez & Primack 2011), modelling the evolution of the luminous components of galaxies has lagged behind due to the intrinsic complexity of gas dynamics and star formation. Early efforts to incorporate baryonic processes into cosmological simulations accounted for gas cooling, but did not include star formation or related feedback effects. These studies found that cooling gas accreted into dark matter haloes would quickly lose angular momentum and fall to the centre of the potential (Katz & Gunn 1991; Navarro & Benz 1991; Navarro & White 1994). The forming objects had disc-like morphologies, but with low specific angular momenta, and with most of the gas residing in a central spheroid rather than a rotationally supported disc, unlike most observed late-type galaxies. It was argued that the efficient angular momentum loss was largely a consequence of the early collapse and formation of protogalactic clouds which were able to efficiently transfer their angular momentum to the dark matter haloes by dynamical and hydrodynamical friction during merger and accretion events.

A large number of subsequent disc formation studies have attempted to diagnose and fix this so-called 'angular momentum catastrophe'. Most proposed solutions are centred around

⋆E-mail: ptorrey@cfa.harvard.edu
†Hubble Fellow.

preventing the gas from cooling and forming stars too efficiently at high redshift. In a simple experiment, Weil, Eke & Efstathiou (1998) showed that if gas cooling is prevented until $z = 1$, stellar discs could form with specific angular momenta consistent with observed spiral galaxies. The two widely advocated mechanisms to mitigate gas overcooling are heating by an ultraviolet (UV) radiation field and feedback associated with star formation. The UV background (Quinn, Katz & Efstathiou 1996; Navarro & Steinmetz 1997; Hoeft et al. 2006) has been shown to inhibit the accretion of cold gas by low-mass haloes, but does not appear to provide a full solution to the angular momentum problem. Star formation with associated feedback has also been identified as a heating mechanism which might prevent early collapse (e.g. Thacker & Couchman 2000, 2001; Maller & Dekel 2002; Abadi et al. 2003; Robertson et al. 2004; Okamoto et al. 2005; Scannapieco et al. 2008) or efficiently remove low angular momentum material (e.g. Governato et al. 2010; Guedes et al. 2011) which allows less centrally concentrated discs to form. Although strong feedback can improve galactic disc formation, it is not immediately clear that this is the only solution to the angular momentum problem or if other numerical artefacts remain adversely affecting the formation of rotationally supported galaxies.

There are some well-studied issues with the standard density formulation of smoothed particle hydrodynamics (SPH) – which is the most commonly employed SPH formulation for cosmological simulation codes – that can cause spurious angular momentum transfer from gas discs. Okamoto et al. (2003) showed that gas discs embedded in a diffuse hot halo would systematically lose angular momentum due to spurious hydrodynamical torques, an effect that is particularly severe at low resolution (see also Commerçon et al. 2008). However, this problem is resolution dependent, and Governato et al. (2004) illustrated this point by presenting disc galaxy formation simulations in a Λ cold dark matter (ΛCDM) context – without invoking strong feedback – to show that angular momentum loss could be substantially reduced by increasing the mass and spatial resolution. Similarly, Kaufmann et al. (2007) used idealized inside-out disc formation simulations to show that while spurious hydrodynamical angular momentum loss dominates at low particle resolutions, using $>10^6$ SPH particles in each simulated galaxy can make the unphysical hydrodynamical torques subdominant.

Unfortunately, the very high resolution criteria specified in Kaufmann et al. (2007) make the near-term feasibility of carrying out full cosmological box simulations with standard SPH poor. As a result, many recent galaxy formation studies have adopted the 'zoom-in' technique, where a single galaxy can be simulated at a very high mass and spatial resolution (e.g. Agertz, Teyssier & Moore 2011; Guedes et al. 2011). Some of these efforts have led to the formation of galaxies that share many properties in common with our own disc-dominated Milky Way. However, Agertz et al. (2011) argued that – even though they were successful in reproducing a Milky Way type disc galaxy – the properties of their simulated galaxies depend heavily on the choice of the star formation threshold, formation efficiently, feedback parameters and other poorly constrained star formation related parameters. Since 'zoom-in' simulations are limited in their scope to one halo at a time, it becomes difficult to judge if the same simulation parameters (e.g. star formation threshold) would validly reproduce the wide range of observed galaxy morphologies or observationally constrained quantities such as the global star formation rate at different redshifts. Therefore, while 'zoom-in' simulations are a very useful numerical tool to understand how individual galaxies form and evolve, it is necessary to perform large cosmological box simulations, where a wide variety of structures should naturally form which can then be compared directly to the wealth of observational galaxy data. Simulations of representative samples of the Universe permit us to test more clearly the impact of poorly constrained simulation parameters on structure formation by exploring the evolution of a full ensemble of galaxies, rather than one individual object. Once it becomes feasible to produce a large ensemble of realistic galaxies in a cosmological context, we will have a powerful tool to address questions about the driving forces behind galaxy morphological evolution that would complement the efforts of 'zoom-in' simulations.

Another issue that exists in standard density SPH is the formation of dense gas 'blobs' (Kaufmann et al. 2006; Kereš & Hernquist 2009; van de Voort et al. 2011; van de Voort & Schaye 2012) that form via numerical thermal instability that occurs in the absence of thermal conductivity (Hobbs et al. 2012). For example, Kaufmann et al. (2006) presented simulations of inside-out disc formation and found a population of dense gas blobs efficiently accreted on to their central forming galaxy. These blobs – which are not found in adaptive mesh refinement (AMR) simulations (Joung, Bryan & Putman 2012) or more modern SPH algorithms where entropy mixing is included via thermal conductivity (Hobbs et al. 2012) – deliver a substantial amount of gas to forming galaxies, making them capable of impacting the structural properties of galactic gas discs (Hobbs et al. 2012; Sijacki et al. 2012).

One way to improve the prospects of carrying out reliable cosmological simulations without relying on substantial increases in available computational power is to improve the accuracy of the hydro solver for a fixed resolution or computational cost. For example, the primary reason for the required high resolution in Kaufmann et al. (2007) is to decrease the importance of spurious hydrodynamical torques that occur at sharp density boundaries between dense galactic gas disc and the surrounding hot gas haloes. However, if one could remove the source of the spurious hydrodynamical torques and improve the thermal mixing properties, then it may be possible to relax the high-resolution criteria to a more attainable level. It is possible that this could be achieved by either modifying the SPH algorithm (e.g. Ritchie & Thomas 2001; Price 2008; Wadsley, Veeravalli & Couchman 2008; Heß & Springel 2010; Read, Hayfield & Agertz 2010; Abel 2011; Hopkins 2012; Saitoh & Makino 2012) or by moving to a grid-based code where these spurious hydrodynamical torques are not expected to occur (e.g. Okamoto et al. 2003). Indeed, in a recent study by Scannapieco et al. (2012) it has been shown for a single galaxy simulated at a high resolution via a zoom-in technique that the choice for the adopted hydro solver can impact the galaxy morphology.

In this paper, we explore the formation of gas discs in two cosmological simulations: one using a traditional density-based SPH formulation as implemented in GADGET (Springel 2005) and one using a novel moving-mesh grid-based hydrodynamical solver as implemented in AREPO (Springel 2010a). Both GADGET and AREPO are massively parallel hydrodynamical simulation codes that use the same gravity solver and subgrid physics, allowing us to isolate the impact of the hydro solver at an equivalent number of initial resolution elements and nearly equivalent computational cost. We study cosmological simulation runs with the two codes and find that the gas disc scale lengths associated with the cold gas discs formed in AREPO are systematically larger than their GADGET counterparts. We discuss the reasons for these differences including the impact of the numerical resolution. The work described here is an extension of the analysis presented in Kereš et al. (2012) which discussed the properties of galaxies and haloes. In this work, we focus specifically

on the properties of gas discs that form within the two simulations and compare their structural properties.

This paper is structured as follows. In Section 2, we summarize the numerical methodology. We then present our results for the gas disc properties in Section 3, and discuss the causes for the differences in Section 4. Finally, we summarize our findings in Section 5.

2 METHODS

We consider the simulations presented in Vogelsberger et al. (2012), which were performed with the cosmological codes GADGET (Springel 2005) and AREPO (Springel 2010a). These simulations follow structure formation in an $L = 20\,\mathrm{Mpc}\,h^{-1}$ box assuming a standard ΛCDM cosmology ($\Omega_\Lambda = 0.73, \Omega_0 = 0.27, h = 0.7, \sigma_8 = 0.8$). The simulations contain $N_{\mathrm{DM}} = 512^3$ dark matter particles and an equivalent number of gas resolution elements at the start of the simulation, giving a mass resolution of $m_{\mathrm{DM}} = 3.722 \times 10^6\,h^{-1}\,\mathrm{M}_\odot$ and $m_{\mathrm{gas}} = 7.444 \times 10^5\,h^{-1}\,\mathrm{M}_\odot$ (note that the gas resolution element mass can change in AREPO due to mass advection across cell boundaries, but all cells maintain a mass within a factor of 2 of this target value). A comoving gravitational softening length of $\epsilon = 1\,h^{-1}$ kpc was used.

2.1 Comparison parameter selection

A central premise for our comparison is that GADGET and AREPO are very similar simulation codes which allows us to hold a large number of simulation parameters and procedures the same. In addition to containing the same gravity solver, the prescriptions for the radiative cooling of gas (Katz, Weinberg & Hernquist 1996), the evolution of the ionizing background radiation field (Faucher-Giguère et al. 2009) and star formation with associated feedback (Springel & Hernquist 2003) are identical. The fundamental difference between the codes lies in their handling of gas hydrodynamics. While GADGET uses a standard density-based SPH technique to evolve the gas, AREPO solves the fluid equations using an exact Riemann solver on a moving unstructured mesh based on a Voronoi tessellation. AREPO has a number of advantages over the standard SPH method due to its ability to e.g. capture shocks more accurately and better resolve fluid instabilities (Springel 2010a,b; Sijacki et al. 2012). In particular, AREPO can handle weak shocks more reliably than standard SPH codes which wash these features out because of the effects of artificial viscosity (see e.g. Keshet et al. 2003). Moreover, with respect to Eulerian AMR codes used in cosmology, AREPO employs a more accurate gravity solver (see e.g. O'Shea et al. 2005) and a spatial refinement that is continuous with the motion of the fluid. Although these traits have been demonstrated in isolated test problems (Springel 2010a; Sijacki et al. 2012), we would like to understand how these numerical effects can impact the evolution of galaxies in cosmological simulations. Furthermore, because the same gravity solver and subgrid physics prescriptions are used, we avoid some of the uncertainties that remain in code comparisons where these are allowed to vary (e.g. Frenk et al. 1999).

For our comparison, we choose to have both codes start from identical initial conditions and have the same initial number of resolution elements ($N_{\mathrm{DM}} = 512^3$, $N_{\mathrm{gas}} = 512^3$). From a practical standpoint, using the same number of initial resolution elements leads to comparable computational cost for the two codes (with the AREPO simulation taking ~30 per cent more CPU time). This is an important consideration because it is the CPU expense which sets limits on the size and complexity of simulations that can be run. However, since the two codes have roughly comparable CPU consumption for the same number of resolution elements, we simply note that neither code has a distinct advantage in this area.

From a more physical standpoint, using the same number of initial resolution elements results in similar mass resolutions between the two codes. For the dark matter component where no inter-particle mass transfer is required, both simulations share identical mass resolutions. For the baryon component, the SPH particles in GADGET have a fixed mass in time while the cells in AREPO have a time-dependent mass due to mass advection to their neighbours when solving the Riemann problem across cell boundaries. We note, however, that we have included a refinement/derefinement scheme that maintains all hydro cells in our AREPO simulation within a factor of 2 of the SPH particle mass in our GADGET simulation (Vogelsberger et al. 2012). As a result, both simulations share similar (although not identical) mass resolutions. As discussed in Vogelsberger et al. (2012), we emphasize that the fixed particle mass in SPH is connected to inaccuracies made in solving the continuity equation, preventing this algorithm from correctly handling mixing.

Since the dark matter components in both simulations evolve similarly (with some potential differences resulting from the influences of the baryon components), the same large-scale structure and halo properties are present in both simulations (Vogelsberger et al. 2012). As a result, we can compare gas discs which reside in a set of matching haloes that are identified as being present in both simulations. Figs 1 and 2 illustrate this point for two matching haloes taken from our simulations. In these nested maps of the projected gas surface density, it can be seen that the distribution of gas on large scales is similar in the two codes (see the leftmost panels of Figs 1 and 2). This is an expected result, as the gas distribution traces the dark matter distribution on large scales. However, as one examines the distribution of gas on galactic scales (as shown in the central and rightmost panels), it becomes clear that there are prominent differences between the two codes. Specifically, while the gas in the GADGET simulation is distributed in a large number of compact and dense clumps, in AREPO gas has a much smoother distribution. Further inspection of Figs 1 and 2 shows that in the central region there are three galaxies – highlighted by red circles – in the process of merging. The effects of their mutual interaction can be seen in the case of AREPO, where tidal features are visible. Although these galaxies are present in GADGET as well, tidal features are much less prominent because the gas is more centrally concentrated and less rotationally supported. Perhaps the most striking finding from Figs 1 and 2 results from a comparison of the galaxy located nearest to the origin in these plots. While this object appears as a smooth, spatially extended disc in AREPO, the same object in GADGET is better described as a featureless blob.

Figs 1 and 2 summarize the motivation for this work. Even though these simulations have been initiated from the same initial conditions, share the same feedback prescriptions and use the same number of initial resolution elements, the detailed morphological properties of the gas distribution on galactic scales can be very different. This is a very important point because it indicates that the hydro solver has a significant impact on the gas properties. While these differences can be fairly easily identified from the gas surface density maps, a primary goal of this paper is to produce a detailed quantitative comparison of the sizes of the gas discs based on a large sample of galaxies matched between the two simulations.

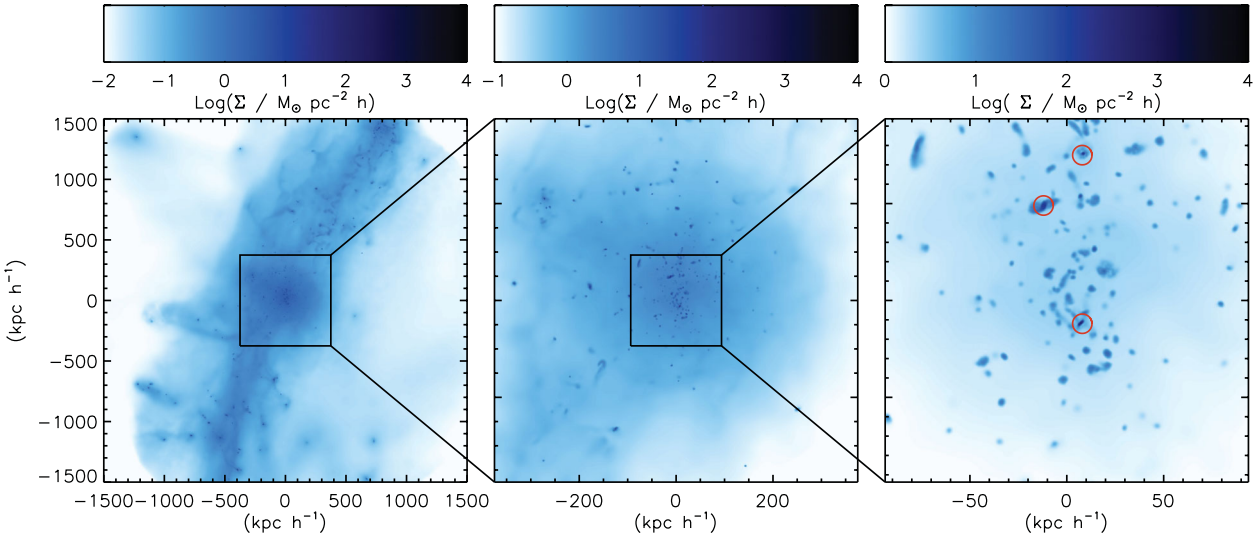

Figure 1. Maps of the projected gas surface density for one object in the GADGET simulation at redshift $z = 1$. The central object has a halo mass $M = 2 \times 10^{12}\,h^{-1}\,\mathrm{M}_{\odot}$. Three nested views are shown to give a clear picture of the gas distribution over a large range of spatial scales. In the rightmost panel, the gas distribution around the central galaxy can be seen to be fairly clumpy and the galaxies themselves appear fairly compact. In this image, three galaxies are in the process of merging, which we have identified with red circles. It is helpful to directly compare this plot to Fig. 2, which shows the same maps for the AREPO simulation.

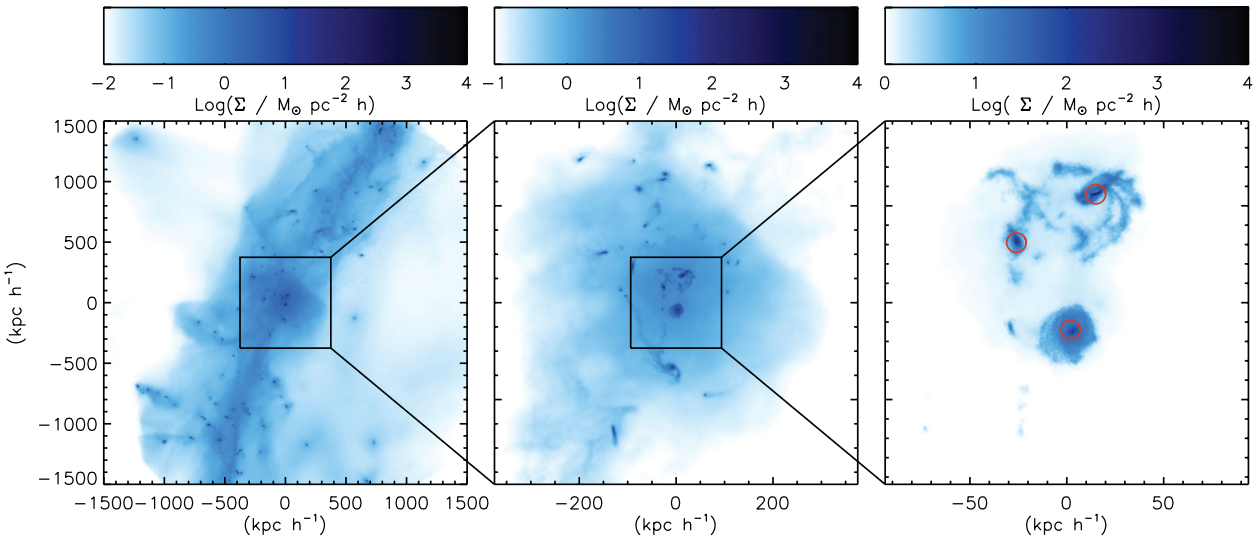

Figure 2. Same as Fig. 1, but for the AREPO simulation. In contrast to Fig. 1, the gas distribution around the central galaxy in the rightmost panel has much fewer gas clumps. The three galaxies that are in the process of merging are highlighted with red circles.

2.2 Gas disc analysis

In what follows, we contrast gas discs that form in the GADGET and AREPO cosmological simulations. To facilitate this comparison, we first identify a sample of matched galaxies from the two simulations. We start by building a catalogue of all structure in each simulation independently using the SUBFIND tool (Springel, White & Hernquist 2001). We assemble a population of 'matching' haloes by finding objects in the GADGET and AREPO simulations that have the same total mass to within 10 per cent and potential minimum locations that are not offset by more than 25 per cent of their half-mass radii. We remove any pairs where the centre of mass is offset by more than $10\,h^{-1}$ kpc from the most tightly bound particle in either halo, as this may be an indication of a merging system. These selection criteria yield 1367 matching haloes in both simulations with total halo masses above $10^{10}\,h^{-1}\,\mathrm{M}_{\odot}$ at $z = 0$. Figs 3 and 4 show examples of the local gas density around a series of five such matching objects in GADGET and AREPO at $z = 0$ and 2, respectively.

In addition to showing differences in the spatial distribution of gas, the gas component of galaxies formed in GADGET and AREPO also differ kinematically. Fig. 5 shows the maps of the gas surface density for an example matched galaxy with vectors indicating the local gas velocity field. Based on the topology of the velocity field, it is evident that the large gas disc in AREPO shows clear rotation about the disc's centre. In contrast, the velocity field of the central galaxy for the same halo in the GADGET simulation exhibits much lower level of circulation.

To analyse the gas disc properties, we identify the gravitationally bound cold and dense gas within each halo. We distinguish the diffuse hot halo from the colder, more dense rotating gas disc by

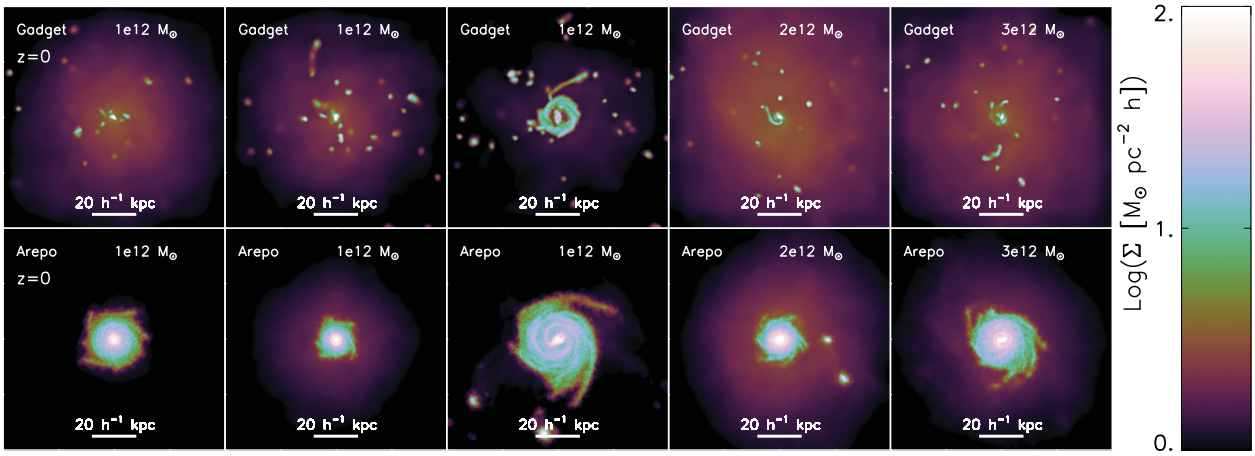

Figure 3. Projected gas surface density maps of five matched objects in GADGET and AREPO chosen at $z = 0$ with host halo masses $\sim 10^{12}\,h^{-1}\,\mathrm{M}_{\odot}$. There are clear differences in the extent of the central gas disc. In addition, the prevalence of dense gas blobs is much higher in the GADGET simulation.

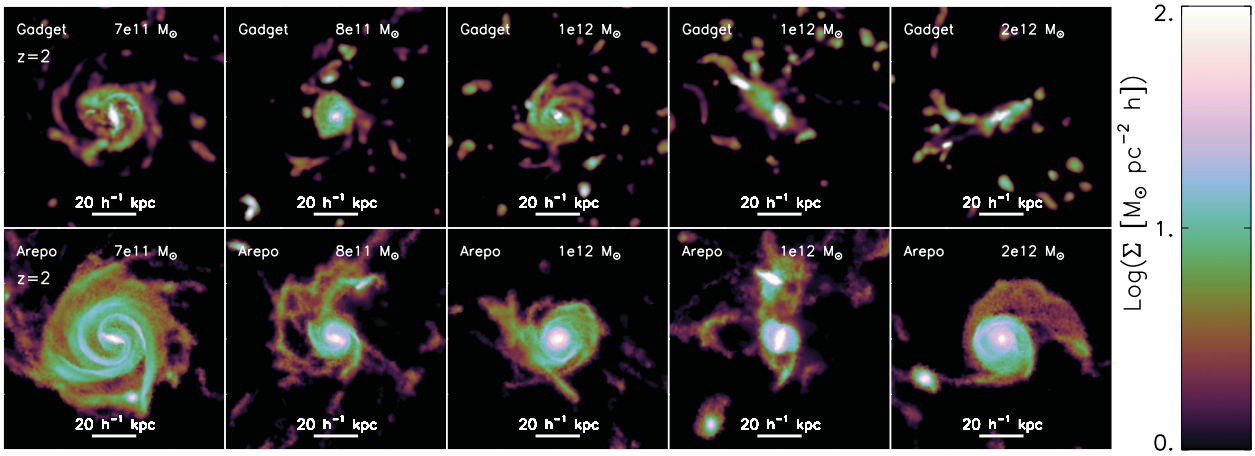

Figure 4. Projected gas surface density maps of five matched objects in GADGET and AREPO chosen at $z = 2$ with host halo masses $\sim 10^{12}\,h^{-1}\,\mathrm{M}_{\odot}$. There are clear differences in the extent of the central gas disc. In addition, the prevalence of dense gas blobs is much higher in the GADGET simulation.

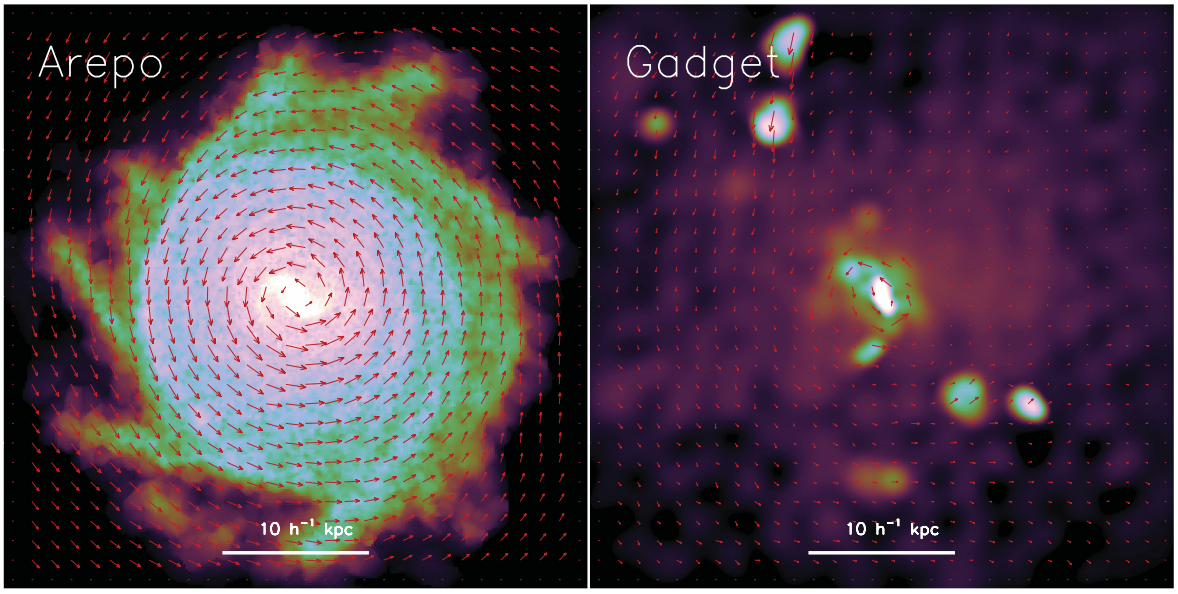

Figure 5. Maps of the projected gas surface density for a typical matched galaxy in a $M_{\mathrm{Halo}} = 10^{12}\,\mathrm{M}_{\odot}$ halo. Red overplotted arrows denote the local gas velocity field. The AREPO galaxy (left-hand panel) is significantly more rotationally supported than its GADGET counterpart (right-hand panel).

making a cut in the $T-\rho$ phase diagram at

$$\log_{10}\left(\frac{T}{[\mathrm{K}]}\right) = 6 + 0.25\log_{10}\left(\frac{\rho}{10^{10}[\mathrm{M}_\odot\ h^2\ \mathrm{kpc}^{-3}]}\right). \quad (1)$$

Our subsequent analysis depends on first removing the hot halo component before measuring the disc surface density profile. However, our results are not very sensitive to this particular cut in the phase diagram (i.e. moving the normalization of this cut up or down by a factor of 5 would not change our conclusions). The remaining cold and dense gas is translated to place the centre of mass at the origin and rotated to align the net gas angular momentum vector in the $\hat{z}$ direction.

Before moving forward, we note that the definition of cold/dense gas cut defined in equation (1) can select material which is not part of the central gas disc. In particular, we find that high-mass haloes in GADGET contain a population of low-mass cold gas clumps which have no associated dark matter overdensity. The rightmost panel in Fig. 1 shows an example of these gas clumps outside of the central object and a similar population of clumps can be found in all massive (i.e. $\sim 10^{12}\,h^{-1}\,\mathrm{M}_\odot$) haloes in the GADGET run. We note that such clumps are also seen in simulations of galaxy formation carried out with other SPH codes (e.g. Okamoto, Nemmen & Bower 2008; Guedes et al. 2011). Most of these clumps are not part of the galactic disc – many of them have entered the halo for the first time, have not yet had any contact with the central galaxy and are on very non-circular trajectories. However, the density and temperature of these clumps allow them to be selected as 'disc mass' according to the definition outlined in equation (1).

In principle, we could remove these cold gas clumps by imposing some additional criteria in our 'disc gas' selection, e.g. we could require disc gas to be on nearly circular trajectories or link together the central disc using a friends-of-friends (FOF) algorithm. Nonetheless, at this point we choose not to impose any additional selection criteria for two reasons. First, we find that deselecting clump material can be sensitive to the details of the clump removal technique that we use. For example, while running an FOF algorithm on the cold and dense gas can efficiently remove clumps that are more than 15 or 20 h^{-1} kpc from the central galaxy, removing the most centrally located gas clumps can depend on our choice for the linking length. Secondly, since these clumps are only present in GADGET, we find that removing them tends to decrease the disc scale lengths obtained for massive GADGET galaxies without having any noticeable impact on the same objects in AREPO. Since one of the conclusions in this paper is that gas discs formed in GADGET are indeed more centrally concentrated than those formed in AREPO, we have tried to avoid any steps in our analysis that could be perceived as artificially pushing us towards that result. Thus, in the following section on gas disc properties, we leave these clumps in our definition of disc mass and save additional discussion about their origin and impact for Section 4.3.

3 DISC COMPARISON

To find the average surface density profile for gas discs, we stack the profiles for all objects in a given halo mass range. A representative set of stacked surface density profiles is shown in Fig. 6. We find the best-fitting exponential profile

$$\Sigma(r) = \Sigma_0\,\exp(-r/R_\mathrm{d}) \quad (2)$$

for each surface density profile via a chi-squared minimization. Note from Fig. 6 that most of the profiles can be fit using a single exponential. However, almost all profiles are distinctly steeper in the inner regions, and this is especially pronounced for GADGET galaxies. This compact central feature is typically associated with a slowly rotating spheroidal component. Since we are primarily interested in the structure of the spatially extended discs and because this inner region is not well resolved in our current simulations (the softening length is $1\,h^{-1}$ kpc comoving, with gravity becoming fully Newtonian after $2.8\,h^{-1}$ kpc, comoving, for the spline softening employed here; Hernquist & Katz 1989), we perform fits by both including and excluding the central $2.8\,h^{-1}$ kpc. We check the quality of each fit by comparing the integral of the best-fitting surface density profile in the fitted region to the true disc mass measured in the simulation. We note that when we exclude the central region all fits for both GADGET and AREPO return the cold, dense gas mass (as defined by equation 2) within 10 per cent, indicating that our prescribed exponential functions are serving as good representations of the actual stacked surface density profiles. When we include the central region, the GADGET fits underestimate the disc mass by ∼20–30 per cent while the AREPO fits underestimate the disc mass by ∼10 per cent. This difference – which is more pronounced for GADGET – is caused by a concentration of material in the central region.

The distribution of best-fitting parameters, Σ_0 and R_d, of the exponential surface density profiles are shown in Fig. 7. We have performed the fits when including (left-hand panel) and excluding (right-hand panel) the central region. We find that the GADGET best-fitting central densities are systematically lowered when we exclude the central region, while the AREPO central densities change less. This is a result of the fact that, on average, GADGET objects contain a larger fraction of their gas in the central region. More importantly, we find that the distribution of disc scale lengths is systematically different between the GADGET and AREPO galaxies, with the AREPO galaxies being described by larger scale lengths regardless of whether we account for the central region. This is a central result of this paper, and confirms the idea that the AREPO discs are larger based on visual inspection of the gas surface density maps. We emphasize that changing the number of galaxies in each stacked surface density profile, the exact normalization of our cold/hot phase boundary cut, or other detailed aspects of the analysis does not affect this conclusion.

Fig. 7 shows clearly the average offset towards larger disc scale lengths for the AREPO gas discs, we find it instructive to show the best-fitting exponential disc scale lengths as a function of host halo mass. Fig. 8 shows the disc scale lengths (including the central $2.8\,h^{-1}$ kpc) as a function of halo mass at redshifts $z = 2$ and 0 in the left- and right-hand panels, respectively. This allows us to see more clearly how the gas discs from the two codes compare to one another at a fixed halo mass. For each bin we show disc scale length values obtained by first stacking the objects and then fitting the exponential surface density profiles (continuous lines), and by computing the median disc scale length from a set of individually fit galaxy surface density profiles (dashed lines). Hatched regions mark 25 and 75 per cent of the distribution for the individually fit profiles. Regardless of the adopted procedure, the AREPO galaxies have larger scale lengths than their GADGET counterparts at both redshifts and for all halo masses. From Fig. 8, it results that the AREPO discs are between 1.5 and 2 times larger than their GADGET counterparts.

We note that for objects with a halo mass $M > 10^{11.5}\,h^{-1}\,\mathrm{M}_\odot$ there is a discrepancy between the disc scale lengths obtained using our stacking procedure with respect to the median disc scale lengths obtained from individual objects in the GADGET simulations. The reason for this discrepancy is the presence of cold gas blobs

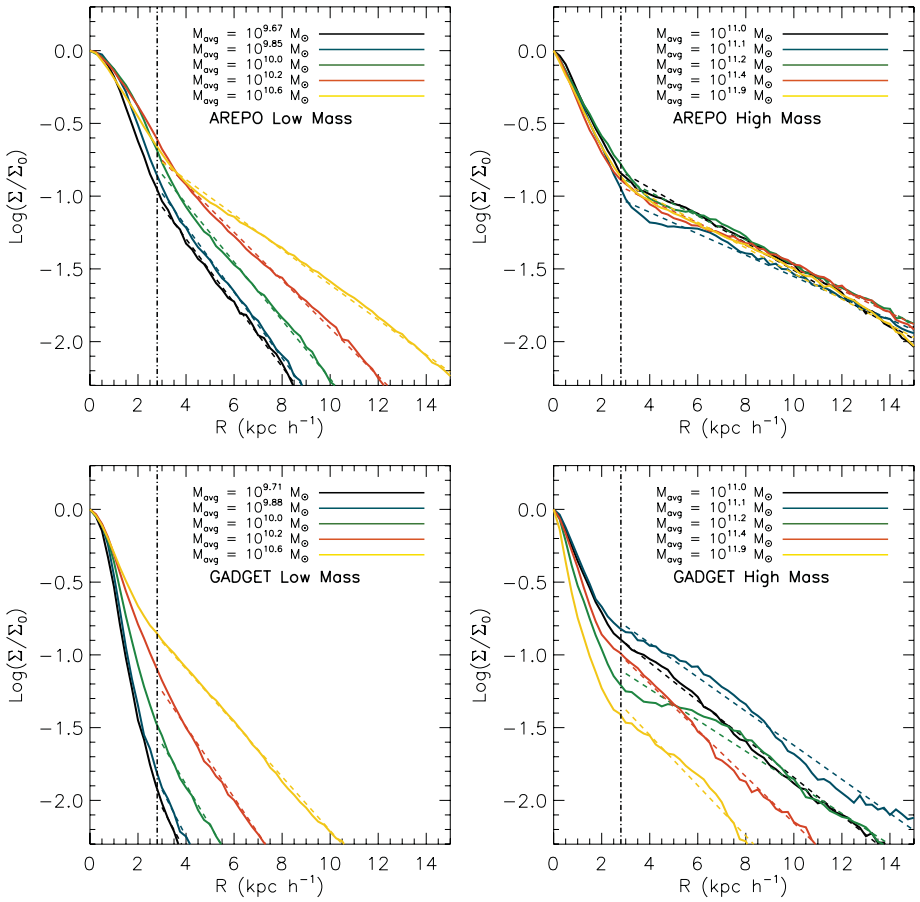

Figure 6. Stacked mass profiles at $z = 0$ for the low-mass AREPO objects (top left), high-mass AREPO objects (top right), low-mass GADGET objects (bottom left) and high-mass GADGET objects (bottom right). The true mass profiles are shown as solid lines, while the best-fitting exponential functions are shown as dashed lines. Each colour corresponds to an average surface density profile for all galaxies in a given halo mass range, with the average halo mass, $M_{\rm avg}$, indicated in the legend. The vertical dot–dashed lines denote the spatial scale over which the gravitational potential is softened, i.e. 2.8 h^{-1} kpc, comoving.

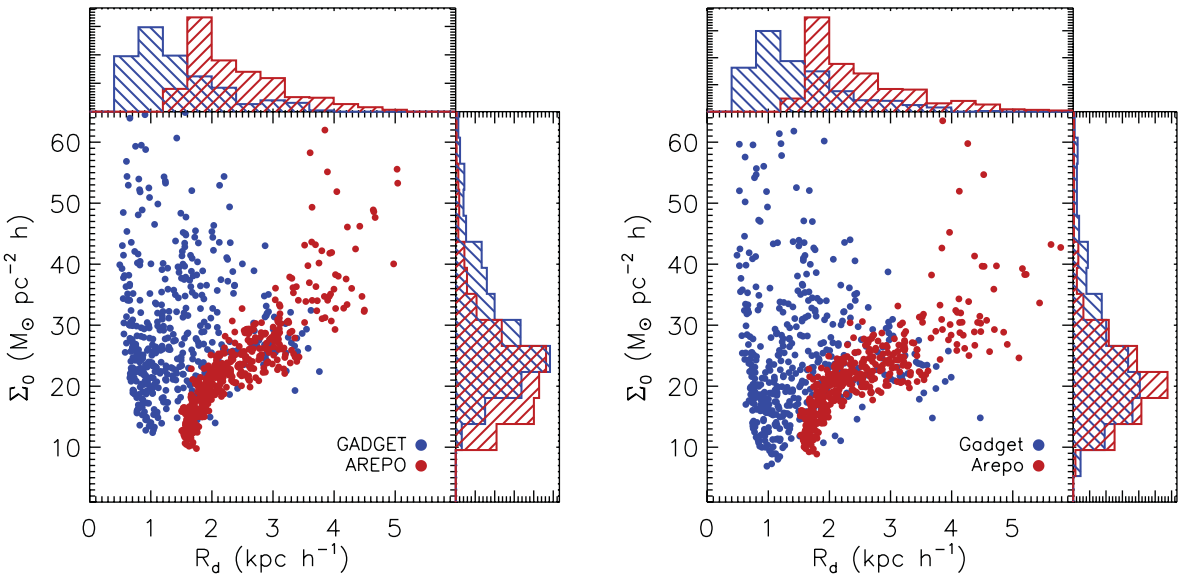

Figure 7. The best-fitting exponential surface density profile parameters to the whole disc (left) and with the central region excluded (right). The distribution of best-fitting parameters for $R_{\rm d}$ and Σ_0 is illustrated in the histograms. Clearly, AREPO objects have larger disc scale lengths than their GADGET counterparts. Including or excluding the central region does not alter this conclusion.

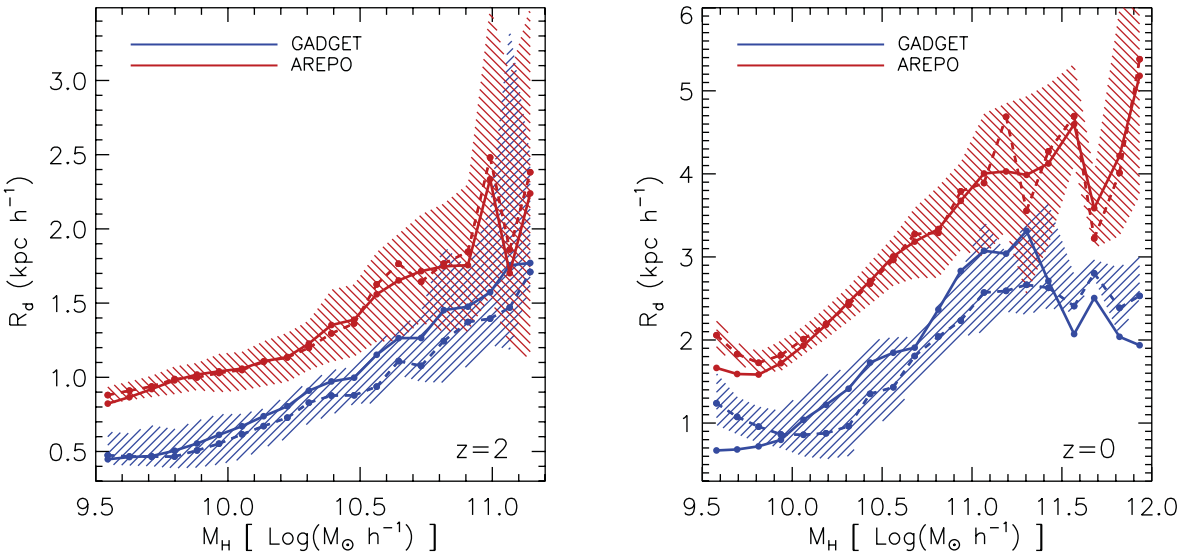

Figure 8. The best-fitting exponential disc scale lengths (in physical units) as a function of halo mass for GADGET and AREPO objects at $z = 2$ (right) and $z = 0$ (left). Continuous lines indicate R_d values for the stacked galaxies in each mass bin, while dashed lines denote the median R_d obtained by fitting exponential profiles to individual objects. Hatched regions are 25 and 75 per cent of the distribution. The AREPO discs are substantially larger at all halo masses and at both redshifts.

surrounding the central gas disc. As discussed in the previous section, since these blobs are cold and dense they are included in our definition of 'disc gas'. Stacking many objects with a large population of blobs can then systematically bias the estimate of the disc scale length. Thus, we note that the apparent trend of the disc scale length with the halo mass at the high-mass end in the GADGET simulations as seen in the lower right-hand panel of Fig. 8 is affected by the presence of cold blobs. For these high-mass systems, the central discs are just not well described by single exponential profiles. An analogous population of cold gas blobs is not present in the AREPO simulation. This is the primary reasons why the solid and dashed lines – representing the stacked best-fitting disc scale length and median of individually fit disc scale lengths – are in better mutual agreement for AREPO galaxies.

Differences between the GADGET and AREPO galaxies can also be seen via a histogram of the gas specific angular momentum, as shown in Fig. 9. In this plot, where the specific angular momentum distribution for the example galaxies illustrated in Fig. 5 is shown, there is a clear distinction between the two codes. The AREPO galaxy shows a narrow distribution around $j_{\rm circ}$ with most of the gas on circular orbits, and thus rotationally supported. The GADGET galaxy instead exhibits a much wider distribution around $j_z/j_{\rm circ} = 1$ due to the significant gas component which is on highly non-circular orbits, with some material even counter-rotating, as evidenced by negative $j_z/j_{\rm circ}$ values.

Fig. 10 shows the specific angular momenta of the gas discs and of all baryons as a function of galaxy baryon mass. The hatched regions indicate where actual spiral and elliptical galaxies are located, as noted by Fall (1983). We have verified that the recent observational sample of Courteau et al. (2007) falls within the hatched region occupied by spirals. We find the specific angular momenta of the cold gas and stellar material in the AREPO simulation to be significantly larger than that of the GADGET objects. The larger specific angular momenta of the AREPO galaxies indicates that they are more rotationally supported, which accounts for their larger disc scale lengths.

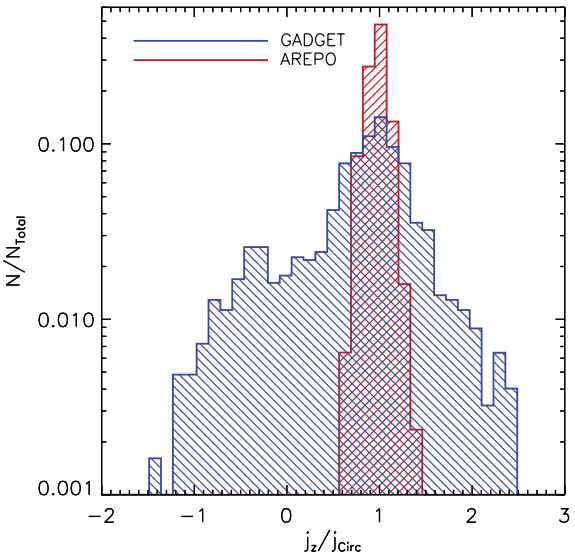

Figure 9. The distribution of specific angular momenta in the disc for a typical matched galaxy in a $M_{\rm Halo} = 10^{12}\,{\rm M}_\odot$ halo. On the x-axis the ratio of the $\hat{z}$-component of the specific angular momentum to the expected specific angular momentum for a particle at that location on a circular orbit is shown. Both codes exhibit distributions that peak about 1, which corresponds to a rotationally supported gas disc. However, while the AREPO disc shows a narrow distribution, with most gas being on nearly circular orbits, the GADGET object has a much wider distribution, with some gas on highly non-circular trajectories.

4 ORIGIN OF THE DISCREPANCIES

In this paper, we have presented a comparison of gas discs formed in cosmological simulations (Vogelsberger et al. 2012) performed with the SPH-based code GADGET and the moving-mesh code AREPO. Both codes use an identical gravity solver and include the same physical processes (e.g. cooling, subgrid model for star formation and feedback), but use fundamentally different hydro solvers. Whereas

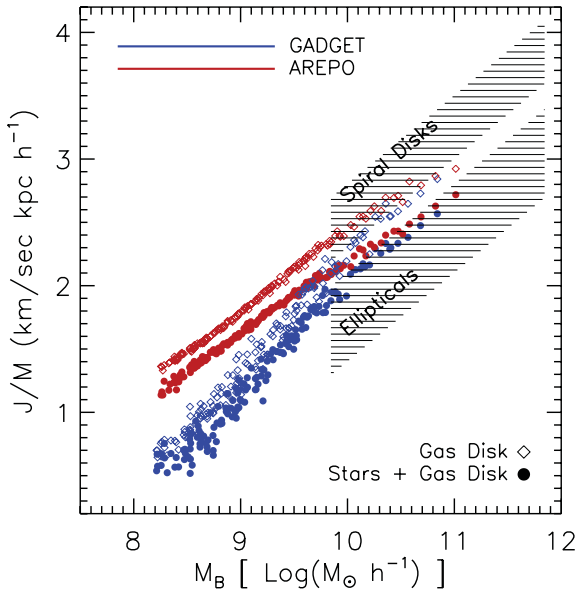

Figure 10. Specific angular momentum as a function of baryon mass for the gas (diamonds) and baryons (filled circles) for the matched sample of AREPO and GADGET galaxies. Hatched regions denote locations of spirals and ellipticals on this diagram as defined by Fall (1983).

GADGET uses an SPH approach to evolve the gas, AREPO uses a finite-volume scheme on a moving Voronoi mesh.

Our primary conclusion is that the cold gas discs that form with AREPO are described by notably different surface density profiles than discs formed using GADGET. We showed that, on average, the cold gas discs in AREPO simulations have significantly larger scale lengths compared to a matched sample of GADGET discs. Consistently, we also find higher specific angular momenta for the AREPO discs. Now that we have identified systematic differences in the disc scale lengths and angular momenta we discuss their principle numerical origins and address ways in which the discrepancies may be reduced.

4.1 Spurious hydrodynamical torques

It is well known that conventional formulations of SPH suffer from artificial angular momentum transport at phase boundaries – like the hot halo cold-disc transition. For example, Okamoto et al. (2003) showed that SPH simulations are prone to angular momentum transfer at this interface and that this can have implications for disc formation in cosmological simulations. Moreover, Okamoto et al. (2003) demonstrated that shearing flows at phase boundaries are more accurately captured in grid-based hydro solvers. Thus, this is one particular area where we expect that the hydro solver included in AREPO should yield more accurate results compared to GADGET.

One solution to this problem is to completely decouple the 'hot' and 'cold' particle neighbour searches (Marri & White 2003; Okamoto et al. 2003). In principle, this modification does a better job at estimating the local gas density using only particles that are in the same phase allowing for a cleaner separation of multiphase gas boundaries. Since this will eliminate all hydrodynamical interactions between the hot and cold phase, the spurious loss of angular momentum will be eliminated. However, decoupling the neighbour searches for particles based on their phase could also lead to artificial suppression of other physical phenomena that rely on direct interaction of multiphase gas such as ram pressure stripping or shock capturing (see e.g. the discussion in Marri & White 2003 for their procedure to address this issue).

Another solution proposed is to increase the simulation resolution substantially (Okamoto et al. 2003; Kaufmann et al. 2007). Increasing the resolution will reduce the influence of the pressure gradient misestimation that occurs at density phase boundaries in standard SPH (see e.g. Agertz et al. 2007). Kaufmann et al. (2007) tested the impact of resolution on idealized inside-out disc formation simulations using SPH and found that by increasing the number of SPH particles in a halo above 10^6 the artificial hydrodynamical angular momentum loss became subdominant to other torquing mechanisms. This problem is less severe (if present at all) in grid-based codes like AREPO where both density phase boundaries and shearing flows are more accurately handled (Okamoto et al. 2003; Agertz et al. 2007; Sijacki et al. 2012). As a result, simulated gas discs in GADGET rapidly lose their angular momentum unless they have a very large number of resolution elements while the same gas discs are able to evolve without such severe angular momentum loss at the same resolution in AREPO.

Since this artificial angular momentum transport is most prominent at low resolution, this is the main reason for the differences seen between the disc scale lengths of GADGET and AREPO objects at relatively low masses (i.e. $<10^{11}\,h^{-1}\,\mathrm{M}_{\odot}$) and will contribute to the loss of angular momentum for higher mass systems (i.e. $<10^{12}\,h^{-1}\,\mathrm{M}_{\odot}$). We note that the most massive haloes considered in our current paper approach the resolution criteria set forth by Kaufmann et al. (2007) (i.e. $\sim 10^6$ particles per halo), so we do not expect spurious hydrodynamical angular momentum loss to be the dominant problem in our high-mass simulated objects. However, for the low-mass objects in our simulation which are by definition more poorly resolved, spurious angular momentum loss is bound to have a substantially larger impact. This conclusion is supported by examining the specific angular momentum content of the GADGET and AREPO galaxies – as shown in Fig. 10 – which demonstrates that the discrepancy between the two codes is larger for low-mass galaxies.

The resolution dependence of spurious hydrodynamical angular momentum transport demonstrated in Kaufmann et al. (2007) implies that increasing the resolution of our GADGET simulations by an appropriate factor (an increase in the number of SPH particles of 10^3 would give us the desired 10^6 particles per halo at the low-mass end) could improve the agreement between GADGET and AREPO. In fact, since massive galaxies are assembled via hierarchically merging smaller objects together, it is necessary to have $>10^6$ SPH particles in all haloes – including low-mass systems – to avoid spuriously losing angular momentum in low-mass systems that will ultimately become part of well-resolved, high-mass galaxies (Kaufmann et al. 2007). This is seemingly in accord with the results of very high resolution 'zoom-in' simulations (e.g. Governato et al. 2004) that have found the angular momentum loss in gas discs formed in standard SPH simulations can be substantially reduced by increasing the particle resolution. However, while the 10^6 SPH resolution elements per halo is a reasonable requirement for 'zoom-in' simulations, this same requirement is not yet feasible for intermediate- and low-mass haloes in full cosmological box simulations. In that sense, we consider it an advantage that grid-based codes such as AREPO do not suffer from this spurious hydrodynamical angular momentum loss even at resolutions well below 10^6 particles per halo.

4.2 Gas heating and cooling

Although GADGET and AREPO share the same prescriptions for radiative gas cooling, non-adiabatic heat sources and mixing at phase boundaries can cause differences in the growth of galactic gas discs. Vogelsberger et al. (2012) presented an analysis of the evolving thermodynamic gas properties in our cosmological simulations. One conclusion from this analysis is that the cooling in AREPO is more efficient than in GADGET, which is driven primarily by differences in the cooling rates of diffuse halo gas. There are two main reasons for the differences in these cooling rates which are discussed in detail in Vogelsberger et al. (2012) and summarized here.

The first reason is differences in dissipative heating in haloes driven by the presence of turbulent energy. Bauer & Springel (2012) performed a comparison of the properties of simulated driven turbulence using GADGET and AREPO and found that while the two codes produce similar velocity and density power spectra for high mach numbers (i.e. for highly supersonic driven turbulence), there are prominent differences in the way turbulent power cascades to smaller scales in the subsonic regime. In AREPO, a Kolmogorov-like turbulent cascade is recovered which transports energy to smaller spatial scales. However, in GADGET, the turbulent large-scale eddies are quickly dissipated close to the cooling radius and transformed into incoherent small-scale velocity noise which is converted into thermal energy as the velocity noise is damped out via artificial viscosity. This heats gas and inhibits cooling in GADGET haloes, driving part of the difference in the cooling rates seen in Vogelsberger et al. (2012).

The second reason stems from differences in mixing between the two codes, especially at density phase boundaries. For low-mass galaxies, the gas cooling time-scale in the halo is relatively short, such that the material is able to cool on to the central galaxy with similar efficiency in both codes. However, for a typical massive galaxy in our simulations, the diffuse halo gas becomes sufficiently hot and the gas cannot cool rapidly due to radiative losses. However, mixing that occurs around infalling substructures as cool gas is hydrodynamically stripped can substantially lower the local cooling time-scale (Marinacci et al. 2010). Idealized tests of gas stripping (Agertz et al. 2007; Sijacki et al. 2012) show that this mixing will be suppressed in GADGET.

A similar mixing boundary layer can develop at the interface of the central gas disc and the diffuse hot halo. This shearing phase boundary can generate mixing via Kelvin–Helmholtz instabilities which will be poorly resolved in GADGET (Okamoto et al. 2003). Although the diffuse halo gas sitting just above the gas disc boundary may have long cooling times, continued efficient hot-mode gas accretion can be facilitated by mixing at this boundary. Sijacki et al. (2012) demonstrated this point by examining the cooling rates of gas in an idealized gas sphere with GADGET and AREPO. They find that the cooling rates are nearly identical when no gas rotation is included, which validates that the cooling prescriptions in both codes are in fact functionally identical. However, when the same test is repeated with gas rotation the cooling rates for the two codes became discrepant, with AREPO cooling more efficiently. The more efficient cooling only sets in once a substantial amount of gas settles into a rotationally supported disc that can interact with the ambient halo gas. Kereš et al. (2012) present evidence for enhanced cooling of this same sort in massive galaxies in the cosmological simulations by noting that the hot haloes in AREPO have cooler cores compared to GADGET and the gas in AREPO tends to be on radially inward trajectories – both of which are consistent with a scenario of less subsonic turbulence dissipation and of increased cooling in a mixing boundary layer between the diffuse halo gas and dense gas disc.

The combined effect of 'extra heating' in GADGET from the poorly resolved turbulent power cascade and 'extra cooling' in AREPO from better resolution of mixing at phase boundaries explain the global thermodynamic differences seen in Vogelsberger et al. (2012). This also explains part of the differences in disc scale lengths that we see in this paper. Notably, high-mass galaxies in AREPO will be more efficient at accreting material from the hot halo at late times which will help them maintain a gas-rich disc.

It is worth noting that several proposals have been put forward to improve the mixing at phase boundaries in SPH, which may bring the two codes into better agreement. For example, it has been suggested that by including a thermal conductivity term contact discontinuities and instabilities can be more accurately handled (e.g. Price 2008; Wadsley et al. 2008), which would improve the mixing picture with respect to the standard SPH. Alternatively, moving away from the density-based formulation of SPH to an energy or pressure formulation can substantially reduce the artificial surface tension at contact discontinuities, which can help to resolve instabilities and mixing with higher accuracy (e.g. Ritchie & Thomas 2001; Saitoh & Makino 2012). In particular, Hopkins (2012) has recently shown how such a formalism can be derived from a variational principle, as in Springel & Hernquist (2002), resulting in a fully conservative version of SPH. Other changes, such as modifying the shape of the adopted smoothing kernel with a substantial increase in the number of neighbours used in the hydro calculations, or modifying the momentum equation evaluated in the code, have all also shown promise in improving the performance of SPH at resolving instabilities (e.g. Read et al. 2010; Abel 2011).

4.3 Cold clumps

One important issue contributing to the differences in the disc scale lengths for high-mass objects in GADGET and AREPO is the efficient accretion of low angular momentum gas via dense clumps. These clumps can be quite easily identified using projected surface density maps of the gas around relatively massive galaxies residing in $\sim 10^{12}\,\mathrm{M}_{\odot}$ haloes in GADGET as is shown in Figs 3 and 4 at $z = 0$ and 2, respectively. In contrast, very few blobs are present in the AREPO galaxies aside from discrete objects which we have identified to be subhaloes with clearly associated dark matter components.

4.3.1 Identifying clump material

We can identify the clump particles by noting that they are overdense relative to the ambient hot halo density, colder than the ambient hot halo temperature and do not have any substantial dark matter overdensity associated with them. To demonstrate this point, Fig. 11 shows a 2D histogram of the material that is part of the primary subhalo (as identified via SUBFIND) in the five matched haloes between 10^{12} and $3 \times 10^{12}\,h^{-1}\,\mathrm{M}_{\odot}$ at $z = 0$ in density–radius space (also shown in Fig. 3). Although the clumps can be as or even more prominent at higher redshifts, here we focus on this mass range and redshift in our analysis for demonstrative purposes.

We can place rough boundaries to break the density–radius space down into three physically meaningful components: central dense gas, diffuse hot halo gas and cold/dense blobs. The central dense gas – which has been the subject of most of this paper – is concentrated

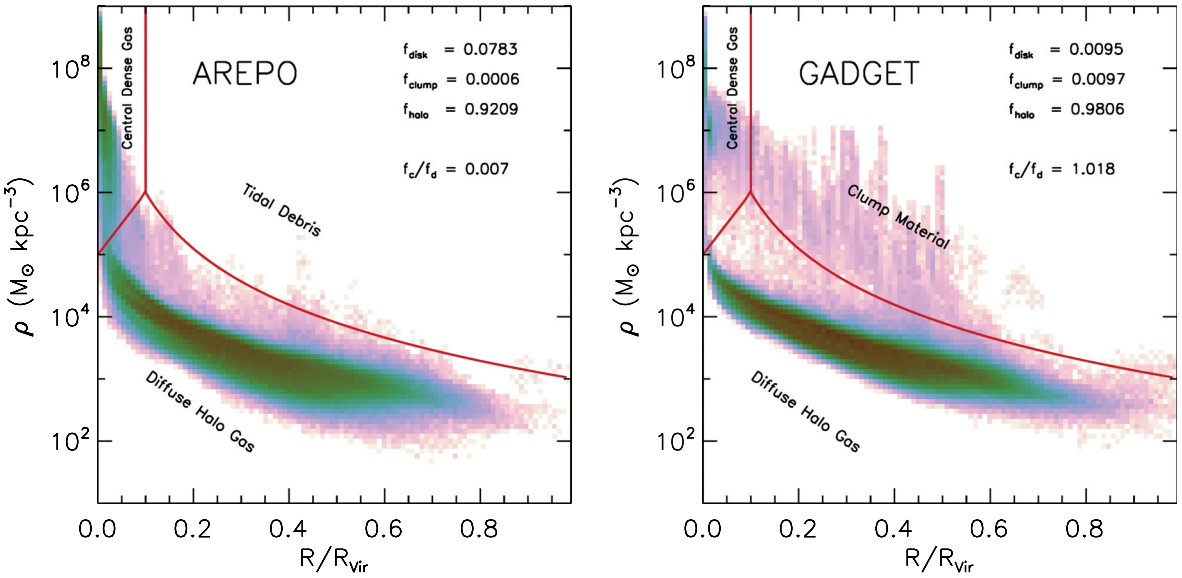

Figure 11. The distribution of gas in the five matched haloes between 10^{12} and $3 \times 10^{12}\,h^{-1}\,\mathrm{M}_\odot$ in AREPO (left) and GADGET (right). Red lines mark the boundaries we have chosen to separate the diffuse halo gas, central dense gas and clump material, and are described in detail in the text. The fraction of gas that resides in the disc, $f_{\rm disc}$, halo, $f_{\rm halo}$, and clump, $f_{\rm clump}$, regions are represented in each panel. Finally, the ratio of the clump gas mass to the disc gas mass, $f_{\rm c}/f_{\rm d}$, is also shown.

into a relatively small region at small radii and has high density

$$M_{\rm disc} = M\left(\frac{r}{R_{\rm vir}} < 0.1, \rho > 10^{\frac{5+r}{(0.1R_{\rm vir})}}\left[\frac{\mathrm{M}_\odot\,h^2}{\mathrm{kpc}^3}\right]\right). \quad (3)$$

The dense clumps are identified as dense material outside of the noted central dense gas region, i.e.

$$M_{\rm clump} = M\left(\frac{r}{R_{\rm vir}} > 0.1, \rho > \frac{10^3}{(r/R_{\rm vir})^3}\left[\frac{\mathrm{M}_\odot\,h^2}{\mathrm{kpc}^3}\right]\right). \quad (4)$$

Finally, we assign all other material to be part of the diffuse hot halo which is characterized by relatively low density.

The fraction of mass that resides in each region is noted in both panels of Fig. 11. In both GADGET and AREPO, over 90 per cent of the gas mass associated with these systems resides in the diffuse halo region. Vogelsberger et al. (2012) and Kereš et al. (2012) analysed the hot halo gas and found that more hot halo gas is present and that the temperature of this gas is hotter in GADGET compared to AREPO. This is consistent with our discussion from the previous section on the increased artificial heating in GADGET and increased mixing induced cooling in AREPO.

The central dense region in AREPO contains about 8 per cent of the total gas mass, compared to about 1 per cent in GADGET. We identify two simple reasons for this difference. First, more gas is able to cool into this region in AREPO for the reasons discussed in the previous section. Secondly, we find that the AREPO galaxies are able to maintain larger amounts of gas in this region because the dense gas resides in a rotationally supported disc with intermediate star formation rates. In contrast, we find that the GADGET galaxies in these massive systems contain most of their gas mass in a very centrally concentrated region with high densities, which efficiently convert the gas supply into stars.

We now turn to the 'clump material' portion of this diagram. As we described earlier, material that resides in this region is far away from the central galaxy, but very dense compared to the ambient halo gas. Interestingly, we find a substantial population of cold clump gas in the GADGET objects that is not found in the AREPO systems. In terms of the fractional mass distribution, ∼1 per cent of the gas mass is in this region for the GADGET systems, while a negligible fraction is in the same region for AREPO objects. Furthermore, of the small gas fraction that does reside in this region for the AREPO objects, most of this material is associated with tidal features or recently stripped cold gas from infalling satellites.

To quickly estimate the potential impact of these clumps on the growth of the central disc, we represent the ratio of clump mass to disc mass in Fig. 11. In GADGET we find that a comparable amount of mass is in the central dense region as in the clump region. In other words, if these clumps are able to efficiently migrate towards the central object – which we will soon argue is the case – then they are capable of contributing a substantial amount of cold, low angular momentum material to the central galaxy. We note that although these quoted fractional mass distributions depend on our choice for the boundary locations shown in Fig. 11, our conclusion that there is a substantial amount of mass in the clump region for the GADGET objects in this mass range is robust to any reasonable changes in the boundary definition.

4.3.2 *Clump associations*

To classify these clumps, we select all overdense particles according to the cut presented in Fig. 11 and group these particles using an FOF algorithm with a linking length of $l = 3\,h^{-1}$ kpc yielding a set of particles belonging to each clump. Each clump then has a well-defined position, velocity and mass.

One quantity of interest is the dark matter overdensity associated with these clumps. Since we have included only material that is bound to the primary halo within our FOF group, we expect that well-defined substructure (e.g. infalling dwarf galaxies) will have already been removed. We can verify that this is the case by checking the dark matter overdensity associated with each clump, and comparing it to the spherically averaged dark matter density at the clump's position. In practice, we do this by finding the volume associated with the Nth nearest dark matter particle from the clump's centre of mass, and compare that to the spherically averaged dark

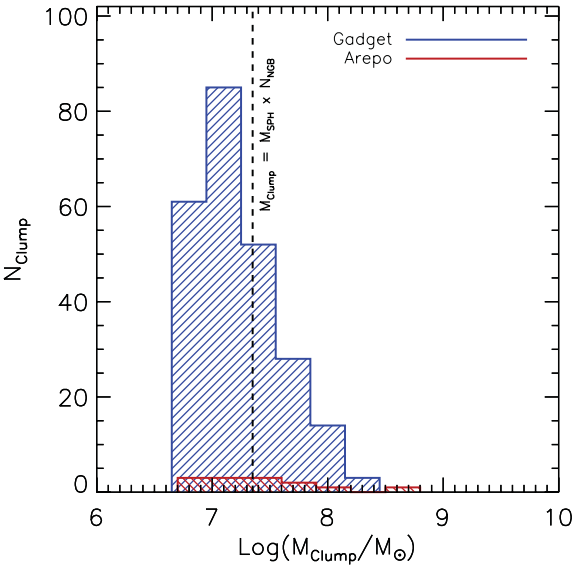

Figure 12. The distribution of clump masses is shown for GADGET (blue) and AREPO (red). We find that there is a substantially larger population of clumps in the GADGET simulation, and that these clumps build up around the mass resolution limit of our simulation which is marked by the vertical dashed line. We emphasize that the few 'clumps' found in the AREPO simulation are actually tidal features or recently stripped cold gas, which are identified as clump material according to our imposed density threshold. The overwhelming majority of the GADGET gas clumps do not contain dark matter and are not associated with infalling substructure or tidal features, as can be gleaned from Figs 1 and 3.

matter density measured in a thin shell at the same radius as of the clump. Although we have verified that this method would allow us to clearly identify substructure, we do not find any clumps in our sample with significant associated dark matter overdensities. We have repeated our overdensity test using $N = 64$, 100, 500 without any change in our results.

The mass spectrum for these blobs is shown in Fig. 12. We find that the majority of the blobs contain just above or below 32 particles, which corresponds to the number of nearest neighbours used in our SPH simulation as denoted by the vertical dashed line in Fig. 12. Clumps tend to build up around the resolution limit of our simulation and as we have verified the mass spectrum changes accordingly if we increase or decrease the number of nearest neighbours. Although we do find a very small number of low-mass cold and dense gas patches in the AREPO simulation, we note that these features are characteristically distinct from the cold gas clumps in GADGET. Specifically, these cold gas patches tend to be associated with tidal features or recently stripped gas from infalling satellites. Therefore, while these cold gas patches meet the density-based selection criteria that we have implemented and do not contain any clearly associated dark matter overdensity, we emphasize that their origin is very different from the large population of cold gas clumps that are seen in the GADGET simulation.

4.3.3 Clump origin and trajectory

The origin of these clumps can be determined by tracing clump particles back in time. We find that the clump particles originate in very mild gas overdensities within the filamentary structures of the intergalactic medium (IGM). As material in these filaments falls into the hot halo environment that surrounds central galaxies in massive objects, mild overdensities are amplified via hydrostatic pressure confinement. We find that the maximum past temperature of the clumps is well below the halo virial temperature, indicating that the blobs did not form via cooling instability of gas overdensities present in the hot halo (as studied in e.g. Kaufmann et al. 2006), but rather remained cold during their accretion from the IGM. This point is demonstrated in Fig. 13 which shows a 2D histogram of the distribution of gas in radius–temperature space for five matched objects with halo masses just above $M = 10^{12}\,h^{-1}\,\mathrm{M}_{\odot}$ at $z = 0$. As labelled within the plot the trajectory for clumps can be readily identified for the GADGET haloes, which allows cold material to migrate from large radii to the central object without ever heating substantially. No analogous migration trajectory exists for the AREPO systems. The clump formation picture we have discussed here is consistent with the clump formation scenario outlined in Kereš et al. (2009), where an analogous population of cold gas clumps were found originating from IGM filaments. Moreover, in agreement with Kereš et al. (2009), we find an accretion rate from these cold clumps in our GADGET simulation of $\dot{M}_{\mathrm{gas}} \sim 0.5\,\mathrm{M}_{\odot}\,\mathrm{yr}^{-1}$ at $z = 0$ for $M = 10^{12}\,h^{-1}\,\mathrm{M}_{\odot}$ systems.

As a clump is gravitationally accelerated towards the halo centre, the clump should begin to be disrupted and mixed via ram pressure stripping and the Kelvin–Helmholtz and Rayleigh–Taylor instabilities. However, it is well known that these instabilities are poorly resolved and that ram pressure stripping is underestimated in the standard density formulation of SPH. In particular, Agertz et al. (2007) and Sijacki et al. (2012) presented numerical experiments that showed cold blobs have artificially long survival times in SPH codes, while grid-based codes like AREPO shred these clumps over substantially shorter time-scales consistent with analytic expectations. As a result, mild overdensities in the accreting filamentary material are condensed and fragmented into a population of high-density cold clumps that have substantially longer survival times in the GADGET simulation compared to AREPO. Since idealized numerical experiments have shown that the survival time-scale for cold gas blobs in GADGET is artificially long compared to analytic expectations, we argue that the survival of these blobs in our GADGET cosmological simulations is a consequence of the same SPH deficiencies.

When the clumps enter the virial radius for the first time, they have non-zero orbital angular momenta about the halo's centre of mass that is consistent with other recently accreted material. However, as the clumps pass through the halo gas, they lose their angular momentum efficiently due to spuriously strong hydrodynamic drag forces (Tittley, Pearce & Couchman 2001) and dynamical friction. This loss of angular momentum puts the clumps on increasingly radial trajectories and allows them to merge with the central object after only one or two orbits. Thus, the clumps become an efficient source of cold, low angular momentum gas feeding the central galaxy.

Fig. 14 specifically highlights the trajectories of a population of clumps in time. A set of cold, dense gas clumps are identified in the leftmost panel of Fig. 14 and their subsequent trajectories are marked with dashed lines in the central and rightmost panels. By inspection of the marked clump trajectories, it can be seen that many clumps move on nearly radial trajectories and eventually merge with the central galaxy. Although each clump has a relatively low mass ($\sim 10^{7}$–$10^{8}\,h^{-1}\,\mathrm{M}_{\odot}$ – see Fig. 12), a sufficiently large number of clumps fall into the central galaxy on a characteristic time-scale of $\sim$1 Gyr. Thus, their cumulative mass amounts to a substantial fraction of the central galaxy gaseous mass. Furthermore, given that they arrive on nearly radial trajectories with low angular

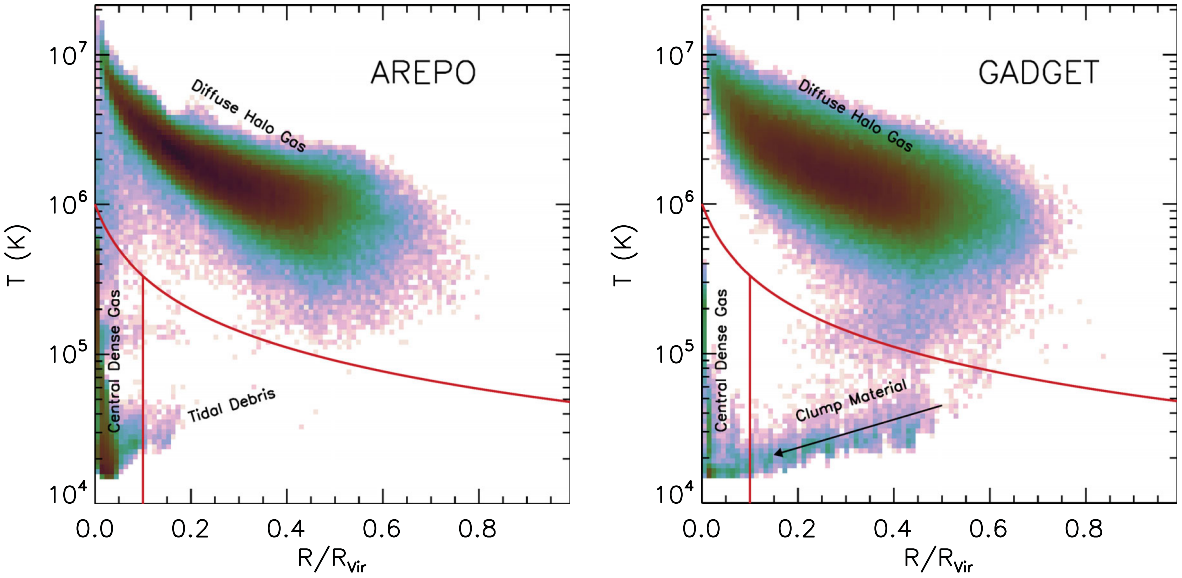

Figure 13. Temperature distribution of bound gas in the five matched haloes between 10^{12} and $3 \times 10^{12}\,h^{-1}\,\mathrm{M}_{\odot}$ in AREPO (left) and GADGET (right). Red lines mark the boundaries we have chosen to separate the diffuse halo gas, central dense gas and clump material.

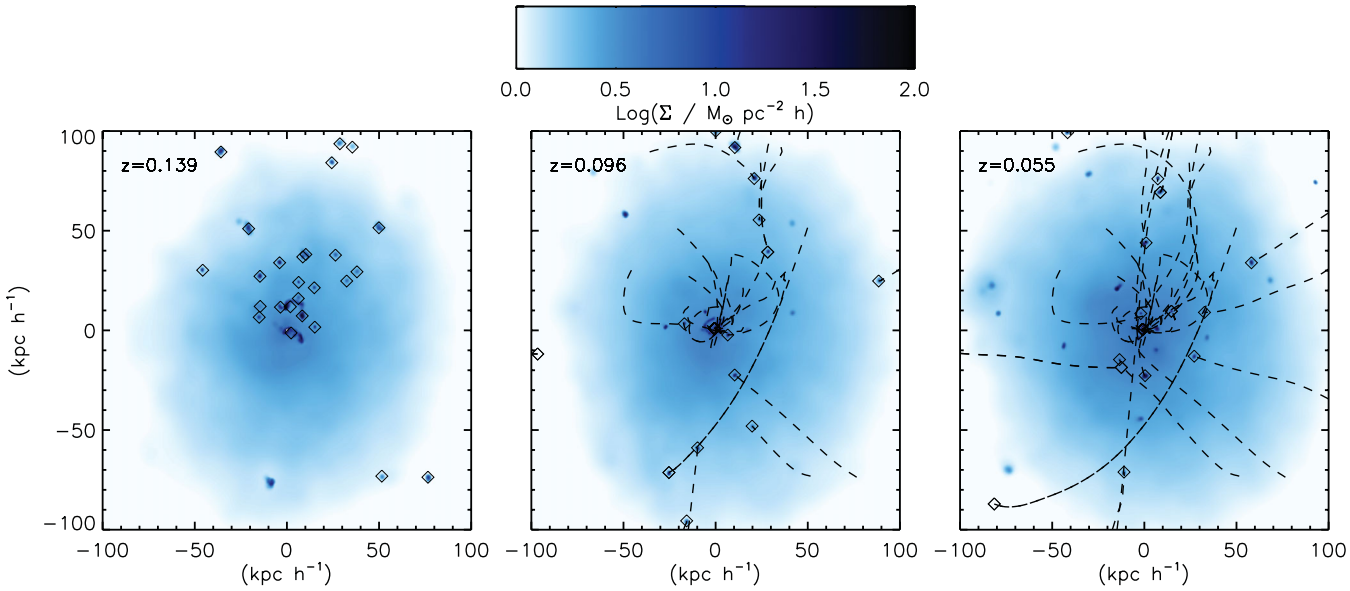

Figure 14. Maps of the gas surface density showing the trajectories of cold, dense gas clumps for a $\sim 10^{12}\,h^{-1}\,\mathrm{M}_{\odot}$ halo in the GADGET simulation at $z = \{0.130, 0.096, 0.055\}$ (left-hand, central and right-hand panels, respectively). A population of clumps (marked with diamond symbols) is identified in the leftmost panel and tracked forward in time. Dashed lines denote their trajectories. The vast majority of the clumps shown are moving towards the central galaxy on nearly radial trajectories, and are able to merge with the central galaxy. Thus, the clumps effectively provide a source of cold, low angular momentum material in the innermost regions, which is of entirely numerical origin.

momentum, the clumps act as an efficient delivery source of low angular momentum fuel to the central galaxy.

A similar population of blobs can be seen in the gas distribution for relatively massive haloes (i.e. $\sim 10^{12}\,h^{-1}\,\mathrm{M}_{\odot}$) in independent studies that used similar versions of GADGET (e.g. Kereš & Hernquist 2009; van de Voort et al. 2011; van de Voort & Schaye 2012). This is an interesting point because the mass resolution used in van de Voort et al. (2011) is about a factor of 2 worse than the resolution used in our present study, and the resolution used in Kereš & Hernquist (2009) is a factor of 7 better. Both of these studies find that these clumps result from fragmented IGM filaments that are able to survive until they merge with the central gas disc. Despite their substantially higher resolution, Kereš & Hernquist (2009) find that these clumps tend to form just above the resolution limit of their simulation – implying a significant change in the clump mass spectrum from what we have found here.

Recently, Hobbs et al. (2012) have made use of a new flavour of SPH (Read & Hayfield 2012) to study the formation and impact of 'blobs' in standard SPH simulations and found their origin to lie in artificial thermal instabilities that can originate from a small number of particles with low entropies with respect to their neighbours. Since the standard formulation of SPH in GADGET lacks any interparticle fluid mixing, these artificial thermal instabilities are allowed to grow and ultimately form a population of dense gas clumps.

Hobbs et al. (2012) show that this artificial thermal instability can be averted by including thermal conductivity (e.g. Price 2008). This issue does not arise with AREPO because cells exchange entropy with their neighbours when mass is advected across cell boundaries, which results in a physically motivated homogenization of the fluid entropy. The presence of these clumps in independent numerical studies of varying resolution (e.g. Kereš & Hernquist 2009; van de Voort et al. 2011; van de Voort & Schaye 2012) seems to imply that these clumps will continue to form and survive at higher resolution even though the specific properties, such as the mass spectrum, will change unless modifications are made to the standard SPH hydro solver.

5 CONCLUSIONS

Here we presented a comparison project aimed at studying the properties of gas discs formed in cosmological simulations performed with two very different hydrodynamical codes – GADGET and AREPO. Our comparison started from an identical set of initial conditions which were evolved forward in time with the two codes which have the same gravity solver and while holding fixed the initial number of resolution elements, and radiative cooling, star formation and feedback prescriptions. However, GADGET and AREPO adopt very different approaches for solving the hydrodynamic equations. While GADGET uses a standard density formulation of SPH, AREPO solves the fluid equations using a Riemann solver on an unstructured moving mesh. In many ways, the hydro solver included in AREPO has accuracy advantages over the SPH solver used in GADGET which can be clearly demonstrated in e.g. idealized shock tube tests, driven turbulence tests and hydro instability tests. The goal of our comparison was to understand the impact of the hydro solver on the formation of gas discs in fully cosmological simulations at a comparable resolution. Our primary conclusions are as follows.

(i) After fitting the gas discs with best-fitting exponential surface density profiles, we find that the AREPO gas discs are systematically larger than their GADGET counterparts. This corresponds to gas discs in GADGET having lower specific angular momentum compared to the matching set of discs formed in AREPO simulation.

(ii) The primary reason responsible for the differences in gas disc scale lengths between the two codes changes as a function of the number of resolution elements and physical environment of the host halo.

(iii) For low-mass objects, low resolution leads to spurious angular momentum transport from the cold disc to the diffuse hot halo in the GADGET simulation. This spurious angular momentum loss is a well-known and documented issue, which can be alleviated by moving to increasingly higher resolution in test problems or 'zoom-in' simulations. However, for large cosmological box simulations, like those we have presented here, the resolution needed to suppress this spurious angular momentum loss is not yet attainable. Grid-based codes – such as AREPO – are not expected to suffer from this same problem and can therefore provide a more accurate answer for the same number of resolution elements and comparable CPU time.

(iv) Poorly resolved subsonic turbulence in GADGET results in dissipative heating of the gas near the cooling radius. This inhibits the accretion of gas on to the central galaxy. In the presence of turbulent energy, AREPO correctly recovers a cascading Kolmogorov-like power spectrum, so no analogous artificial heating source is present.

(v) For high-mass objects, the cooling time-scale of hot halo gas can become comparable to the Hubble time which effectively shuts off fresh gas accretion. However, mixing at density phase boundaries – such as the interface between the cold gas disc and the hot halo – can substantially increase the gas cooling rates. This allows for more gas to cool on to the disc in AREPO given that the mixing at phase boundaries is suppressed in GADGET.

(vi) For high-mass objects, the efficient delivery of low angular momentum gas in the form of cold gas clumps causes the central gas discs in GADGET to be much more centrally concentrated than in AREPO. These clumps form from fragmented IGM filaments and rapidly migrate to the potential minimum as they lose their angular momentum to hydrodynamic drag against the ambient hot halo. The absence of these blobs in AREPO is attributed to the efficient disruption of clumps via ram pressure stripping and the Kelvin–Helmholtz and Rayleigh–Taylor instabilities – all of which are poorly handled in GADGET.

ACKNOWLEDGMENTS

We thank Elena D'Onghia for helpful suggestions on this work and Stéphane Courteau for providing observational data in tabulated form. We thank the anonymous referee for helpful comments on this manuscript. DS acknowledges NASA Hubble Fellowship through grant HST-HF-51282.01-A. LH has been supported in part by NASA ATP award NNX12AC67G.

REFERENCES

Abadi M. G., Navarro J. F., Steinmetz M., Eke V. R., 2003, ApJ, 597, 21
Abel T., 2011, MNRAS, 413, 271
Agertz O. et al., 2007, MNRAS, 380, 963
Agertz O., Teyssier R., Moore B., 2011, MNRAS, 410, 1391
Bauer A., Springel V., 2012, MNRAS, 423, 2558
Boylan-Kolchin M., Springel V., White S. D. M., Jenkins A., Lemson G., 2009, MNRAS, 398, 1150
Commerçon B., Hennebelle P., Audit E., Chabrier G., Teyssier R., 2008, A&A, 482, 371
Courteau S., Dutton A. A., van den Bosch F. C., MacArthur L. A., Dekel A., McIntosh D. H., Dale D. A., 2007, ApJ, 671, 203
Fall S. M., 1983, in Athanassoula E., ed., Proc. IAU Symp. 100, Internal Kinematics and Dynamics of Galaxies. Reidel, Dordrecht, p. 391
Faucher-Giguère C.-A., Lidz A., Zaldarriaga M., Hernquist L., 2009, ApJ, 703, 1416
Fosalba P., Gaztañaga E., Castander F. J., Manera M., 2008, MNRAS, 391, 435
Frenk C. S. et al., 1999, ApJ, 525, 554
Governato F. et al., 2004, ApJ, 607, 688
Governato F. et al., 2010, Nat, 463, 203
Guedes J., Callegari S., Madau P., Mayer L., 2011, ApJ, 742, 76
Heß S., Springel V., 2010, MNRAS, 406, 2289
Hernquist L., Katz N., 1989, ApJS, 70, 419
Hobbs A., Read J., Power C., Cole D., 2012, arXiv e-prints
Hoeft M., Yepes G., Gottlöber S., Springel V., 2006, MNRAS, 371, 401
Hopkins P. F., 2012, preprint (arXiv:1206.5006)
Joung M. R., Bryan G. L., Putman M. E., 2012, ApJ, 745, 148
Katz N., Gunn J. E., 1991, ApJ, 377, 365
Katz N., Weinberg D. H., Hernquist L., 1996, ApJS, 105, 19
Kaufmann T., Mayer L., Wadsley J., Stadel J., Moore B., 2006, MNRAS, 370, 1612
Kaufmann T., Mayer L., Wadsley J., Stadel J., Moore B., 2007, MNRAS, 375, 53
Kereš D., Hernquist L., 2009, ApJ, 700, L1
Kereš D., Katz N., Fardal M., Davé R., Weinberg D. H., 2009, MNRAS, 395, 160
Kereš D., Vogelsberger M., Sijacki D., Springel V., Hernquist L., 2012, MNRAS, 425, 2027

Keshet U., Waxman E., Loeb A., Springel V., Hernquist L., 2003, ApJ, 585, 128
Klypin A. A., Trujillo-Gomez S., Primack J., 2011, ApJ, 740, 102
Maller A. H., Dekel A., 2002, MNRAS, 335, 487
Marinacci F., Binney J., Fraternali F., Nipoti C., Ciotti L., Londrillo P., 2010, MNRAS, 404, 1464
Marri S., White S. D. M., 2003, MNRAS, 345, 561
Navarro J. F., Benz W., 1991, ApJ, 380, 320
Navarro J. F., Steinmetz M., 1997, ApJ, 478, 13
Navarro J. F., White S. D. M., 1994, MNRAS, 267, 401
Okamoto T., Jenkins A., Eke V. R., Quilis V., Frenk C. S., 2003, MNRAS, 345, 429
Okamoto T., Eke V. R., Frenk C. S., Jenkins A., 2005, MNRAS, 363, 1299
Okamoto T., Nemmen R. S., Bower R. G., 2008, MNRAS, 385, 161
O'Shea B. W., Nagamine K., Springel V., Hernquist L., Norman M. L., 2005, ApJS, 160, 1
Price D. J., 2008, J. Comput. Phys., 227, 10040
Quinn T., Katz N., Efstathiou G., 1996, MNRAS, 278, L49
Read J. I., Hayfield T., 2012, MNRAS, 422, 3037
Read J. I., Hayfield T., Agertz O., 2010, MNRAS, 405, 1513
Ritchie B. W., Thomas P. A., 2001, MNRAS, 323, 743
Robertson B., Yoshida N., Springel V., Hernquist L., 2004, ApJ, 606, 32
Saitoh T. R., Makino J., 2012, preprint (arXiv:1202.4277)
Scannapieco C., Tissera P. B., White S. D. M., Springel V., 2008, MNRAS, 389, 1137
Scannapieco C. et al., 2012, MNRAS, 423, 1726
Sijacki D., Vogelsberger M., Kereš D., Springel V., Hernquist L., 2012, MNRAS, 424, 2999
Springel V., 2005, MNRAS, 364, 1105
Springel V., 2010a, MNRAS, 401, 791
Springel V., 2010b, ARA&A, 48, 391
Springel V., Hernquist L., 2002, MNRAS, 333, 649
Springel V., Hernquist L., 2003, MNRAS, 339, 289
Springel V., White M., Hernquist L., 2001, ApJ, 549, 681
Springel V. et al., 2005, Nat, 435, 629
Teyssier R. et al., 2009, A&A, 497, 335
Thacker R. J., Couchman H. M. P., 2000, ApJ, 545, 728
Thacker R. J., Couchman H. M. P., 2001, ApJ, 555, L17
Tittley E. R., Pearce F. R., Couchman H. M. P., 2001, ApJ, 561, 69
van de Voort F., Schaye J., 2012, MNRAS, 423, 2991
van de Voort F., Schaye J., Booth C. M., Haas M. R., Dalla Vecchia C., 2011, MNRAS, 414, 2458
Vogelsberger M., Sijacki D., Keres D., Springel V., Hernquist L., 2012, MNRAS, 425, 3024
Wadsley J. W., Veeravalli G., Couchman H. M. P., 2008, MNRAS, 387, 427
Weil M. L., Eke V. R., Efstathiou G., 1998, MNRAS, 300, 773

This paper has been typeset from a TEX/LATEX file prepared by the author.